Synthesis of Carboxylic Acid-Modified [FeFe]-Hydrogenase Model Complexes Amenable to Surface Immobilization

Christine M. Thomas, Olaf Rüdiger, Tianbiao Liu, Cody E. Carson, Michael B. Hall, and Marcetta Y. Darensbourg*

Department of Chemistry, Texas A&M University, College Station, Texas 77843

Received April 5, 2007

Model complexes of [FeFe]-hydrogenase bearing carboxylic acid functionalities have been designed for applications toward immobilization of hydrogen production electrocatalysts on amino-functionalized carbon electrode surfaces. Using carboxylic acid-substituted thiols, complexes incorporating the −COOH moiety into the thiolate linkers have been synthesized: (μ-$SCH_2CH_2COOH)_2[Fe(CO)_3]_2$ (**1**) and the previously known (μ-$(SCH_2)_2CHCOOH)[Fe(CO)_3]_2$ (**2**). Carboxylic acid units have also been introduced via ligand substitution with a tricarboxyethyl phosphine to generate (μ-pdt)$[Fe(CO)_3][Fe(CO)_2\{P(C_2H_4COOH)_3\}]$ (**3**). To mimic the linkage of complexes of these types to amino-functionalized monolayers, it has been demonstrated that **2** can be coupled with aniline in solution to generate (μ-$(SCH_2)_2CHCONHPh)[Fe(CO)_3]_2$ (**4**), and the stability of this linkage has been addressed. The carboxylic acid-substituted complex **2** undergoes ligand substitution with PMe_3 to generate (μ-$(SCH_2)_2CHCOOH)[Fe(CO)_2(PMe_3)]_2$ (**5**). Complex **5** can then be protonated in either methanol or tetrahydrofuran solvent to generate (μ-$(SCH_2)_2CHCOOMe)(\mu$-H)$[Fe(CO)_2(PMe_3)]_2\}PF_6$ (**6**) and (μ-$(SCH_2)_2CHCOOH)(\mu$-H)$[Fe(CO)_2(PMe_3)]_2\}PF_6$ (**7**), respectively, demonstrating that a range of carboxy-functionalized complexes can be synthesized. Structural characterization and cyclic voltammetry of these complexes indicate that the carboxylic acid functionality has little effect on the structure and reactivity of the diiron dithiolate core.

Introduction

In biology, the reduction of protons to form dihydrogen ($2H^+ + 2e^- \leftrightarrows H_2$) is reversibly catalyzed by the hydrogenases.[1] These enzymes employ bimetallic active sites featuring dithiolate bridged [FeFe] or [NiFe] scaffolds.[2] While electrocatalytic hydrogen production can be accomplished at a platinum electrode, platinum metal is far too expensive and limited in supply to be of practical use in a global hydrogen-based fuel cell economy. For this reason, researchers have examined the attachment of the hydrogenase enzymes to electrodes by either surface adsorption[3] or covalent linkage[4] to assess the electrocatalytic proton reduction and hydrogen oxidation abilities of the enzymes.

Since the structure of [FeFe]-hydrogenase, [FeFe]-H_2ase, was reported,[5] small-molecule Fe_2S_2 model complexes that closely resemble the enzyme's active site have been scrutinized in efforts to better understand the mechanism of stepwise proton reduction in binuclear catalytic sites. The model complexes, based on the well-known organometallics, (μ-$SR)_2[Fe(CO)_2L]_2$,[6] feature two dithiolate-bridged Fe^I centers and as many as six carbonyl ligands. Carbonyl substitution chemistry and variation of the dithiolate linkers has led to a large number of reported [FeFe]-H_2ase model complexes in recent years.[7] Various Fe_2S_2 complexes have been shown to be competent electrocatalysts for the production of hydrogen at fairly negative potentials in the presence of weak acids.[8] Optimization of electrocatalysis by the diiron models has included introduction of hydrophilic ligands such as PTA (phosphatriazaadamantane)[9] and electroactive ligands such as the N-heterocyclic carbene IMes (1,3-

* Corresponding author. E-mail: marcetta@mail.chem.tamu.edu.

(1) (a) Adams, M. W. W.; Stiefel, E. I. *Science* **1998**, *282*, 1842−1843. (b) Cammack, R.; Frey, M.; Robson, R. *Hydrogen as a Fuel: Learning from Nature*; Taylor and Francis: London, 2001.

(2) (a) Adams, M. W. W.; Stiefel, E. I. *Curr. Opin. Chem. Biol.* **2000**, *4*, 214−220. (b) Evans, D. J.; Pickett, C. J. *Chem. Soc. Rev.* **2003**, *32*, 268−275. (c) Darensbourg, M. Y.; Lyon, E. J.; Smee, J. J. *Coord. Chem. Rev.* **2000**, *206*−*207*, 533−561.

(3) (a) Vincent, K. W.; Cracknell, J. A.; Parkin, A.; Armstrong, F. A. *Dalton Trans.* **2005**, 3397−3403. (b) Leger, C.; Jones, A. K.; Roseboom, W.; Albracht, S. P. J.; Armstrong, F. A. *Biochemistry* **2002**, *41*, 15736−15746.

(4) Rüdiger, O.; Abad, J. M.; Hatchikian, E. C.; Fernandez, V. M.; De Lacey, A. L. *J. Am. Chem. Soc.* **2005**, *127*, 16008−16009.

(5) (a) Nicolet, Y.; Piras, C.; LeGrand, P.; Hatchikian, C. E.; Fontecilla-Camps, J. C. *Structure* **1999**, *7*, 13−23. (b) Peters, J. W.; Lanzilotta, W. N.; Lemon, B. J.; Seefeldt, L. C. *Science* **1998**, *282*, 1853−1858.

(6) (a) Reihlen, H.; Gruhl, A.; Hessling, G. *Liebigs Ann. Chem.* **1929**, *472*, 268. (b) Seyferth, D.; Womack, G. B.; Archer, C. M.; Dewan, J. C. *Organometallics* **1989**, *8*, 430−442.

(7) (a) Lyon, E. J.; Georgakaki, I. P.; Reibenspies, J. H.; Darensbourg, M. Y. *J. Am. Chem. Soc.* **2001**, *123*, 3268−3278. (b) Lawrence, J. D.; Li, H.; Rauchfuss, T. B.; Benard, M.; Rohmer, M.-M. *Angew. Chem., Int. Ed.* **2001**, *40*, 1768−1771. (c) Razavet, M.; Davies, S. C.; Hughes, D. L.; Pickett, C. J. *Chem. Commun.* **2001**, 847−848. (d) Tard, C.; Liu, X.; Ibrahim, S. K.; Bruschi, M.; De Gioia, L.; Davies, S. C.; Yang, X.; W. L.-S.; Sawers, G.; Pickett, C. J. *Nature* **2005**, *433*, 610−613. (e) Justice, A. K.; Zampella, G.; De Gioia, L.; Rauchfuss, T. B.; van der Vlugt, J. I.; Wilson, S. R. *Inorg. Chem.* **2007**, *46*, 1655−1664. (f) van der Vlugt, J. I.; Rauchfuss, T. B.; Whaley, C. M.; Wilson, S. R. *J. Am. Chem. Soc.* **2005**, *127*, 16012−16013.

(8) (a) Gloaguen, F.; Lawrence, J. D.; Rauchfuss, T. B. *J. Am. Chem. Soc.* **2001**, *123*, 9476−9477. (b) Chong, D.; Georgakaki, I. P.; Mejia-Rodriguez, R.; Sanabria-Chinchilla, J.; Soriaga, M. P.; Darensbourg, M. Y. *J. Chem. Soc., Dalton Trans.* **2003**, 4158−4163. (c) Capon, J.-F.; Gloaguen, F.; Schollhammer, P.; Talarmin, J. *J. Electroanal. Chem.* **2004**, *566*, 241−247. (d) Jiang, S.; Liu, J.; Shi, Y.; Wang, Z.; Åkermark, B.; Sun, L. *Dalton Trans.* **2007**, 896−902. (e) Morvan, D.; Capon, J.-F.; Gloaguen, F.; Le Goff, A.; Marchivie, M.; Michaud, F.; Schollhammer, P.; Talarmin, J.; Yahouanc, J.-J.; Pichon, R.; Karvarec, N. *Organometallics* **2007**, *26*, 2042−2052. (f) Duan, L.; Wang, M.; Li, P.; Na, Y.; Wang, N.; Sun, L. *Dalton Trans.* **2007**, 1277−1283.

(9) Mejia-Rodriguez, R.; Chong, D.; Reibenspies, J. H.; Soriaga, M. P.; Darensbourg, M. Y. *J. Am. Chem. Soc.* **2004**, *126*, 12004−12014.

10.1021/om7003354 CCC: $37.00
Publication on Web 07/04/2007

Chart 1

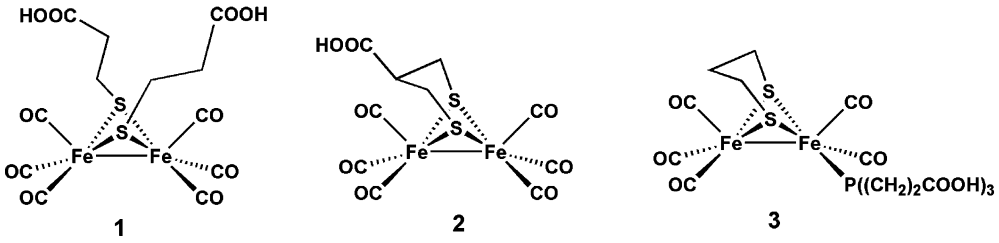

bis(2,4,6-trimethylphenyl)imidazol-2-ylidene).[10] While the mild conditions of nature (H_2 production at pH = 7 and $E = -0.4$ V (vs NHE)) are yet to be achieved, various imaginative approaches to a workable molecular electrocatalyst continue to address the goal. To be of practical use, chemical tethers that achieve immobilization on cheap electrode materials, most likely graphite, must also be developed and their stability assessed. With this goal in mind, Pickett and co-workers recently reported some initial steps toward incorporating model complexes of the active site of [FeFe]-hydrogenase into electrode-bound electropolymeric materials.[11] Our approach utilizes a particularly versatile method for generating amine monolayers on carbon electrodes via electrochemical reduction of aryl diazonium salts developed by Saveant and co-workers.[12] Covalent amide linkages can be formed between such monolayers and molecules bearing a carboxylic acid functionality. With this in mind, the complexes shown in Chart 1, derivatized with carboxylic acid functionalities suitable for attachment to amino-functionalized electrode surfaces via carbodiimide-promoted acylation, have been prepared. In a proof of principle, one of these complexes has been coupled with aniline and the stability of the amido linkage explored.

Two strategies have been employed to prepare model complexes with carboxylic acid functionalities. The first of these incorporates a carboxylic acid group into the thiolate linkage of the Fe_2S_2 complexes (Chart 1), making use of both monodentate thiolate and chelating dithiolate bridging linkers. Complex **2** and an amido derivative of it have been reported by Volkers, Rauchfuss, and Wilson in a study of the coordination properties of dihydroasparagusic acid or $(HSCH_2)_2CHCO_2H$ in diiron carbonyl and nickel derivatives.[13] The second approach is via substitution of a CO ligand with a carboxy-substituted phosphine. It is important to note that it has previously been demonstrated that functionalized dithiolate linkers can be used to covalently attach diiron complexes to electrode surfaces,[14] and functionalized dithiolates and phosphines have been used to link diiron complexes to photosensitizers.[15]

Scheme 1

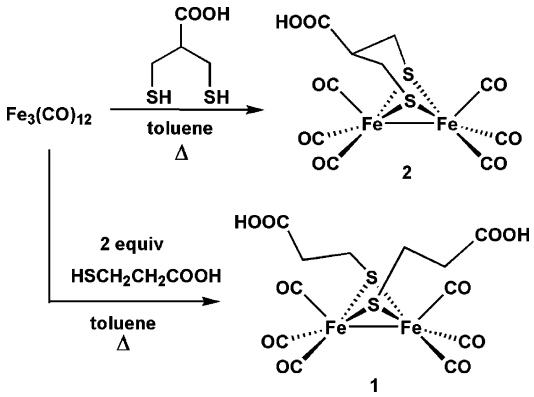

Results and Discussion

Synthesis and Characterization. Access to the carboxythiolate-bridged complexes was achieved using routes similar to those previously employed for simple alkyl thiolates.[16] Refluxing a toluene solution of 3-mercaptopropionic acid and $Fe_3(CO)_{12}$ results in formation of red-orange $(\mu\text{-}SCH_2CH_2COOH)_2[Fe(CO)_3]_2$ (**1**), isolated in 35% yield (Scheme 1). Complex **1** is insoluble in most organic solvents and unstable to highly polar solvents such as acetonitrile, DMF, and methanol; however, satisfactory ESI-MS, combustion analysis, and IR data confirmed its identity. Like other $(\mu\text{-}RS)_2[Fe(CO)_3]_2$ complexes,[8b] the IR spectrum of **1** has diagnostic ν(CO) stretching frequencies at 2071(m), 2037(s), and 1994(s) cm^{-1}, with an additional band at 1735(w) cm^{-1} for the carboxylic acid moiety (Table 1).

The 2-carboxy-1,3-propanedithiol[17] and red $(\mu\text{-}(SCH_2)_2CHCOOH)[Fe(CO)_3]_2$ (**2**)[13] were prepared following literature protocols. Shorter heating periods contributed to greater yields of **2** (Scheme 1). The ν(CO) bands in the IR spectrum of **2** are consistent with those of the parent $(\mu\text{-pdt})[Fe(CO)_3]_2$ complex (Table 1), with an additional stretch observed at 1730 cm^{-1} for the −COOH moiety. The ^1H NMR spectrum (298 K, acetone-d_6) of complex **2** contains three diagnostic signals for the protons on the propanedithiolate linker, indicative of the inequivalence of the axial and equatorial protons of the iron dithiacyclohexane rings. Similar behavior has been observed in the low-temperature ^1H NMR spectrum of $(\mu\text{-pdt})[Fe(CO)_3]_2$,[7a] and in the case of **2**, it is likely that substitution at the 2-position of the propanedithiolate hinders ring interconversion.

Incorporation of a carboxylic acid into the diiron dithiolate model complexes through substitution of a CO ligand with a carboxy-functionalized phosphine has been used by Sun et al. to generate $(\mu\text{-pdt})[Fe(CO)_3][Fe(CO)_2(Ph_2PCH_2COOH)]$ and $(\mu\text{-}(SCH_2)_2NC_3H_7[Fe(CO)_3][Fe(CO)_2(Ph_2PCH_2CH_2COOH)]$.[18] For

(10) Tye, J. W.; Lee, J.; Wang, H.-W.; Mejia-Rodriguez, R.; Reibenspies, J. H.; Hall, M. B.; Darensbourg, M. Y. *Inorg. Chem.* **2005**, *44*, 5550−5552.

(11) Ibrahim, S. K.; Liu, X.; Tard, C.; Pickett, C. J. *Chem. Commun.* **2007**, 1535−1537.

(12) (a) Delamar, M.; Hitmi, R.; Pinson, J.; Saveant, J. M. *J. Am. Chem. Soc.* **1992**, *114*, 5883−5884. (b) Allongue, P.; Delamar, M.; Desbat, B.; Fagebaume, O.; Hitmi, R.; Pinson, J.; Saveant, J. M. *J. Am. Chem. Soc.* **1997**, *119*, 201−207.

(13) Volkers, P. I.; Rauchfuss, T. B.; Wilson, S. R. *Eur. J. Inorg. Chem.* **2006**, 4793−4799.

(14) Vijaikanth, V.; Capon, J.-F.; Gloaguen, F.; Schollhammer, P.; Talarmin, J. *Electrochem. Commun.* **2005**, *7*, 427−430.

(15) (a) Ekström, J.; Abrahamsson, M.; Olson, C.; Bergquist, J.; Kaynak, F. B.; Eriksson, L.; Sun, L.; Becker, H.-C.; Åkermark, B.; Hammarström, L.; Ott, S. *Dalton Trans.* **2006**, 4599−4606. (b) Wolpher, H.; Borgström, M.; Hammarström, L.; Bergquist, J.; Sundström, V.; Styring, S.; Sun, L.; Åkermark, B. *Inorg. Chem. Commun.* **2003**, *6*, 989−991.

(16) Winter, A.; Zsolnai, L.; Huttner, G. *Z. Naturforsch.* **1982**, *37b*, 1430−1436.

(17) Singh, R.; Whitesides, G. M. *J. Am. Chem. Soc.* **1990**, *112*, 1190−1197.

(18) Dong, W.; Wang, M.; Wang, F.; Jin, K.; Yu, Z.; Sun, L. personal communication.

Table 1. Infrared Spectroscopic Data for Complexes 1−6 (in acetonitrile) as Well as Some Unfunctionalized Fe_2S_2 Complexes for Comparison

complex	$\nu(CO)_{Fe}$ (cm^{-1})	$\nu(C{=}O)$ (cm^{-1})	ref
(μ-$SCH_2CH_2COOH)_2[Fe(CO)_3]_2$ (**1**)[a]	2071(m), 2037(s), 1994(s)	1735	*b*
(μ-$SEt)_2[Fe(CO)_3]_2$	2073(m), 2038(vs), 1992(s)		7a
(μ-$(SCH_2)_2CHCOOH)$ $[Fe(CO)_3]_2$ (**2**)[a]	2077(m), 2034(s), 1992(s), 1978(sh)	1730	*b*
(μ-pdt) $[Fe(CO)_3]_2$	2074(m), 2036(vs), 1995(s)		7a
(μ-pdt)$[Fe(CO)_3][Fe(CO)_2\{P(CH_2CH_2COOH)_3\}]$ (**3**)	2041(s), 1981(s), 1966(sh), 1922(w)	1733	*b*
(μ-pdt) $[Fe(CO)_3][Fe(CO)_2(PMe_3)]$	2037(s), 1980(s), 1919(m)		19
(μ-$(SCH_2)_2CHCONHPh)[Fe(CO)_3]_2$ (**4**)	2078(m), 2038(s), 1997(s)	1690, 1600	*b*
(μ-$(SCH_2)_2CHCOOH)[Fe(CO)_2(PMe_3)]_2$ (**5**)[a]	1984(m), 1948(vs), 1903 (s)	1729	*b*
(μ-pdt) $[Fe(CO)_2(PMe_3)]_2$)	1979(m), 1942(s), 1898(s)		20
$\{(\mu$-$(SCH_2)_2CHCOOH)$ (μ-H) $[Fe(CO)_2(PMe_3)]_2\}PF_6$ (**6**)	2034(s), 1994(s)	1739	*b*
$\{(\mu$-pdt)(μ-H) $[Fe(CO)_2(PMe_3)]_2\}PF_6$	2029(s), 1989(s)		20

[a] Spectrum recorded in tetrahydrofuran. [b]This work.

our purposes, the commercially available phosphine $P(CH_2CH_2COOH)_3HCl$ was chosen in order to maximize the potential for eventual surface attachment through amido linkages. Addition of this phosphine to (μ-pdt)$[Fe(CO)_3]_2$ in acetonitrile in the presence of 1 equiv of the decarbonylation agent $ONMe_3$ leads to formation of $(CO)_3Fe(\mu\text{-pdt})Fe(CO)_2\{P(C_2H_4COOH)_3\}$ (**3**) in 80% yield. Complex **3** is characterized by a ^{31}P NMR signal at 52.9 ppm, and, similar to other monophosphine Fe_2S_2 complexes, the IR spectrum of **3** features stretches at 2041(s), 1981(s), 1966 (sh), and 1922 (w) cm^{-1} for the iron carbonyls. A band at 1733 cm^{-1} is assigned to the C═O of the carboxylic acids.

Coupling of Carboxy-Functionalized Diiron Dithiolates to Amines in Solution. To mimic the linkage of the carboxylic acid-substituted diiron complexes with surface-bound monolayers of aniline, complex **2** was coupled with aniline in solution to generate the corresponding amide complex. Addition of aniline to complex **2** in the presence of diisopropylcarbodiimide as a coupling agent results in rapid formation of (μ-$(SCH_2)_2$-$CHCONHPh)[Fe(CO)_3]_2$ (**4**) in high yield (Scheme 2).[21] The structure of amide **4** was confirmed by X-ray crystallography (*vide infra*). The IR spectrum of complex **4** is similar to that of **2** with the exception of the disappearance of the $\nu(C{=}O_{OH})$ stretch at 1730 cm^{-1} and the appearance of two new bands at 1690 and 1600 cm^{-1} attributed to the amide functionality. An analogous carboxamido derivative, (μ-$(SCH_2)_2CHCONHEt)[Fe$-$(CO)_3]_2$, is reported to have bands at 1660 and 1563 cm^{-1}.[13]

For electrode-supported catalytic applications, the stability of the carboxylic amide tether under various conditions is of obvious importance. Specifically, it is crucial that this linkage be stable at negative potentials (*vide infra*) and under moderately acidic conditions. To assess this stability, complex **4** was exposed to 10 equiv of acetic acid in THF solution and monitored by IR spectroscopy for 48 h. No change was observed in either the $\nu(C{\equiv}O_{Fe})$ or $\nu(C{=}O_{NHR})$ bands under these conditions. Likewise, complex **4** was found to be stable to 10 equiv of HCl for at least several hours. Exposure to larger excesses of strong acid (dissolution in a 1:1 mixture of concentrated HCl(aq) and THF) resulted in gradual decomposition of complex **4**, as indicated by bleaching of the solution's color and formation of brown solids over the course of 1 h. Even in the absence of acid, at temperatures higher than 60 °C, gradual decomposition of complex **4** occurs. After 2 h of heating in toluene, the IR spectrum revealed a decrease in the intensity of the $\nu(C{=}O_{NHR})$ stretch at 1690 cm^{-1} and the appearance of a new broad stretch around 1730 cm^{-1}.

Ligand Substitution and Protonation of (μ-$(SCH_2)_2CHCOOH)$-$[Fe(CO)_3]_2$ (2). While the Fe^IFe^I carbonyl derivatives **1**, **2**, and **3** are suitable for catalytic proton reduction at an electrode surface, a carboxy-substituted complex suitable for the reverse reaction (dihydrogen oxidation) is also desirable. In the [FeFe]-H_2ase enzyme as well as in the diiron model complexes, requirements for H_2 uptake are (1) oxidized iron to achieve d^6 Fe^{II} and (2) an open site for H_2 binding and activation. Previously, it was shown that protonation of the disubstituted phosphine complex (μ-pdt)$[Fe^I(CO)_2(PMe_3)]_2$ leads to the cationic $Fe^{II}(\mu\text{-H})Fe^{II}$ complex.[20] Under photolysis to remove a CO ligand, this oxidized complex and its analogues are active toward H_2 uptake, as has been assayed by their ability to facilitate H/D exchange reactions in D_2/H_2O mixtures.[20,22] For potential applications toward electrocatalytic hydrogen oxidation chemistry, such ligand substitution and protonation reactions have been pursued using the carboxy-substituted complex **2**.

Reaction of complex **2** with 2 equiv of PMe_3 at 50 °C for several hours resulted in the formation of the disubstituted complex (μ-$(SCH_2)_2CHCOOH)[Fe(CO)_2(PMe_3)]_2$, complex **5**, in ca. 80% yield.[23] The IR spectrum of complex **5** is consistent with that reported earlier and in good agreement with that of (μ-pdt)$[Fe(CO)_2(PMe_3)]_2$, whose solid-state structure found the PMe_3 ligands to be in basal positions on each square-pyramidal iron and *transoid* to each other.[20] Complex **5** has diagnostic ^{31}P NMR signals at 27.6 and 21.5 ppm. This inequivalence of the two phosphorus atoms, observed only at the low temperature, stopped-exchange region, in (μ-pdt)$[Fe(CO)_2(PMe_3)]_2$ (at 29.6 and 25.7 ppm),[22] likely arises from the fixed position of the chair/boat iron dithiacyclohexane conformers even at room temperature upon incorporation of the carboxylic acid moiety of **5**. Isomeric forms due to phosphine positions (axial/basal) on individual iron centers is typically indicated by a difference in ^{31}P NMR chemical shift positions of over 10 ppm.[22]

Under the conditions reported for protonation of (μ-pdt)$[Fe$-$(CO)_2(PMe_3)]_2$ (conc HCl, MeOH),[22] complex **5** can be proto-

Scheme 2

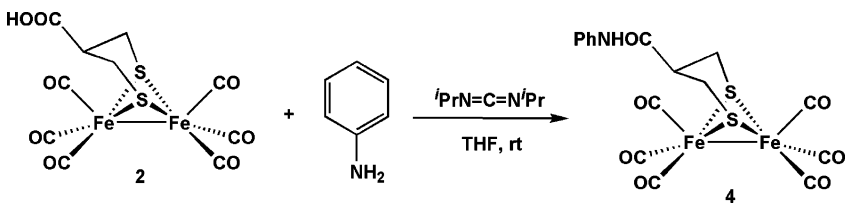

Table 2. Electrochemical Reduction Potentials (vs ferrocene) of Complexes 1−5[a]

complex	E_{pc}[b] $Fe^IFe^I \rightarrow Fe^IFe^0$	E_{pc}[b] $Fe^IFe^0 \rightarrow Fe^0Fe^0$
(μ-$SCH_2CH_2COOH)_2[Fe(CO)_3]_2$ (**1**)	−1.73 V	−2.37 V
(μ-$(SCH_2)_2CHCOOH)[Fe(CO)_3]_2$ (**2**)	−1.64 V	−2.51 V
(μ-pdt)[$Fe(CO)_3$][$Fe(CO)_2${$P(CH_2CH_2COOH)_3$}] (**3**)[b]	−2.07 V	−2.44 V
(μ-$(SCH_2)_2CHCONHPh)[Fe(CO)_3]_2$ (**4**)	−1.67 V	−2.60 V
(μ-$(SCH_2)_2CHCOOH)[Fe(CO)_2(PMe_3)]_2$ (**5**)[c]	−2.42 V	

[a] CO-saturated CH_3CN solution (0.1 M $^nBu_4NBF_4$) with a glassy carbon working electrode ($A = 0.071$ cm^2) referenced to Cp_2Fe/Cp_2Fe^+ as an internal standard. Counter electrode: Pt. Scan rate: 200 mV/s. [b] See discussion on assignments in text. [c] Under Ar atmosphere.

nated to generate a hydride-bridged $Fe^{II}Fe^{II}$ complex; however, concomitant esterification of the carboxylic acid moiety occurs, producing {(μ-$(SCH_2)_2CHCOOMe)(\mu$-H)[$Fe(CO)_2(PMe_3)]_2$}PF_6 (**6**) in 76% yield. Infrared spectroscopy of **6** reveals two ν(CO) stretches at 2034 and 1994 cm^{-1} and a stretch at 1739 cm^{-1} for the C(═O)OMe moiety. Protonation of **5** with HCl in THF rather than methanol results in an $Fe^{II}Fe^{II}$ hydride complex with conservation of the −COOH group, and {(μ-$(SCH_2)_2CHCOOH)$-(μ-H)[$Fe(CO)_2(PMe_3)]_2$}PF_6 (**7**) can be isolated in 54% yield. The ^{1}H NMR spectra of **6** and **7** both feature a diagnostic hydride resonance at −15.2 ppm with a $^2J_{H-P}$ coupling constant of 22 Hz (for (μ-H)(μ-pdt)[$Fe(CO)_2(PMe_3)]_2^+$, $\delta = -15.2$ ppm and $^2J_{H-P} = 22$ Hz).[22] The ^{31}P NMR spectra of **6** and **7** feature two distinct PMe_3 signals (23.9 and 21.7 ppm for **6**; 25.1 and 21.8 for **7**). Again the small difference reflects the slightly different chemical environment of the two PMe_3 ligands derived from the locked position of the μ-$(SCH_2)_2$CHCOOMe bridge. A septet at −142.7 ppm is assigned to the PF_6^- counteranion.

Solution Electrochemistry. In order to realize the ultimate goal of converting solution electrocatalysts to electrode surface-supported catalysts, it is important to establish that the incorporation of tethers does not dramatically affect the redox behavior of the diiron complexes. For this purpose, cyclic voltammetry data were collected for complexes **1**−**7** for comparison with the analogous unfunctionalized complexes.[24] The cyclic voltammogram (CV) of the well-studied (μ-pdt)-$[Fe(CO)_3]_2$ displays two reduction events at −1.74 V (quasi-reversible) and −2.35 V (irreversible) versus the ferrocene/ferrocenium couple.[8b] [*Note: Previous studies reported these redox events relative to the NHE in attempts to relate potentials of the model complexes to the hydrogenase enzyme. The uncertainty of standards in nonaqueous solvents leads to a reconsideration and to the simpler protocol used here. Addition of the 0.40 V conversion factor*[25] *converts the Fc/Fc*$^+$ *referenced values to the NHE values reported earlier*.] The CVs of complexes **1**, **2**, and **4** were recorded in CO-saturated CH_3CN solution, as these conditions give the most well-defined redox waves for related compounds.[8b] Reduction potentials under these conditions are listed in Table 2. CVs of the carboxylic acid complexes **1** and **2** and the carboxyamido complex **4** essentially

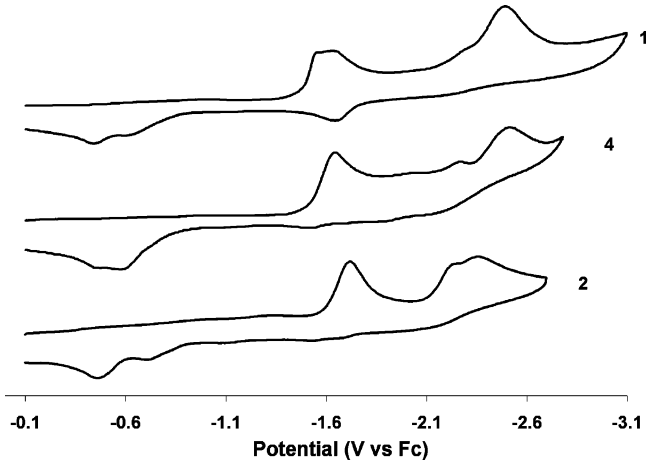

Figure 1. Cyclic voltammograms of complexes **1**, **2**, and **4** (2.5 mM in 0.1 M $^nBu_4NBF_4$ in MeCN, under CO atmosphere).

feature two irreversible reductive processes (Figure 1).[26] The first reduction events at −1.73, −1.64, and −1.67 V for complexes **1**, **2**, and **4**, respectively, can be assigned as the one-electron $Fe^IFe^I \rightarrow Fe^IFe^0$ reduction on the basis of previous assignments for the unfunctionalized complexes.[8b] Unlike the (μ-pdt)$[Fe(CO)_3]_2$ parent, this reduction event is irreversible even when more negative potentials are not applied or when the scan rate is increased. An additional one-electron reduction, which on the basis of the (μ-pdt)$[Fe(CO)_3]_2$ parent may be assigned as $Fe^IFe^0 \rightarrow Fe^0Fe^0$, is also observed at −2.37 V for **1**, −2.51 V for **2**, and −2.60 V for **4**. Complexities in the reductive region of the CVs of simpler compounds have elicited detailed electrochemical, spectroelectrochemical, and computational study.[27] Heinekey and co-workers reported that chemical reduction of complexes of this type leads to a bimolecular decomposition pathway involving Fe−S bond cleavage and the production of tetrairon species with propanedithiolate spanning two diiron units.[28] Clearly the carboxylate moiety introduces even more possibilities for complications in the compounds of our current study.

Figure 2 displays the cyclic voltammogram of acetic acid in MeCN, showing a broad response centered at −2.6 V that shows a linear dependence on HOAc concentration. As expected, complexes **1**, **2**, and **4** also have reductive events in this region, likely due to the carboxylate moiety. In the presence of increasing concentrations of acetic acid ($pK_a = 22.6$),[29] the current height of the first reductive wave remains relatively constant for complexes **1**, **2**, and **4**, indicating that the Fe^IFe^0

(19) Li, P.; Wang, M.; He, C.; Li, G.; Liu, X.; Chen, C.; Åkermark, B.; Sun, L. *Eur. J. Inorg. Chem.* **2005**, 2506−2513.

(20) Zhao, X.; Georgakaki, I. P.; Miller, M. L.; Yarbrough, J. C.; Darensbourg, M. Y. *J. Am. Chem. Soc.* **2001**, *123*, 9710−9711.

(21) Monitoring this reaction by ^{1}H NMR spectroscopy (acetone-d_6) reveals quantitative conversion of the −COOH to −CONHPh within 15 min. Isolated yields are lower as a result of difficulties separating the amide product from carbodiimide-derived side products.

(22) Zhao, X.; Georgakaki, I. P.; Miller, M. L.; Mejia-Rodriguez, R.; Chiang, C.-Y.; Darensbourg, M. Y. *Inorg. Chem.* **2002**, *41*, 3917−3928.

(23) A similar reaction was observed previously (ref 13) using the deprotonated carboxylate derivative NR_4{(μ-pdt-COO^-)$[Fe(CO)_3]_2$} to generate NR_4{(μ-pdt-COO^-)$[Fe(CO)_2(PMe_3)]_2$}.

(24) The reduction potentials of complexes **2** and **5** have been previously reported (ref 13).

(25) Gagné, R. R.; Koval, C. A.; Lisensky, G. C. *Inorg. Chem.* **1980**, *19*, 2854−2855.

(26) Additional features in the CV of complexes **1** and **2** likely arise from the redox activity of the carboxylic acid moiety itself. A CV of 2-carboxy-1,3-propanedithiol is included in the Supporting Information.

(27) Cheah, M. H.; Borg, S. J.; Best, S. P. *Inorg. Chem.* **2007**, *46*, 1741−1750.

(28) Aguirre de Carcer, I.; DiPasquale, A.; Rheingold, A. L.; Heinekey, D. M. *Inorg. Chem.* **2006**, *45*, 8000−8002.

(29) Izutsu, K. *Acid-Base Dissociation Constants in Dipolar Aprotic Solvents*; Blackwell Scientific Publications: Oxford, 1990; Vol. 35.

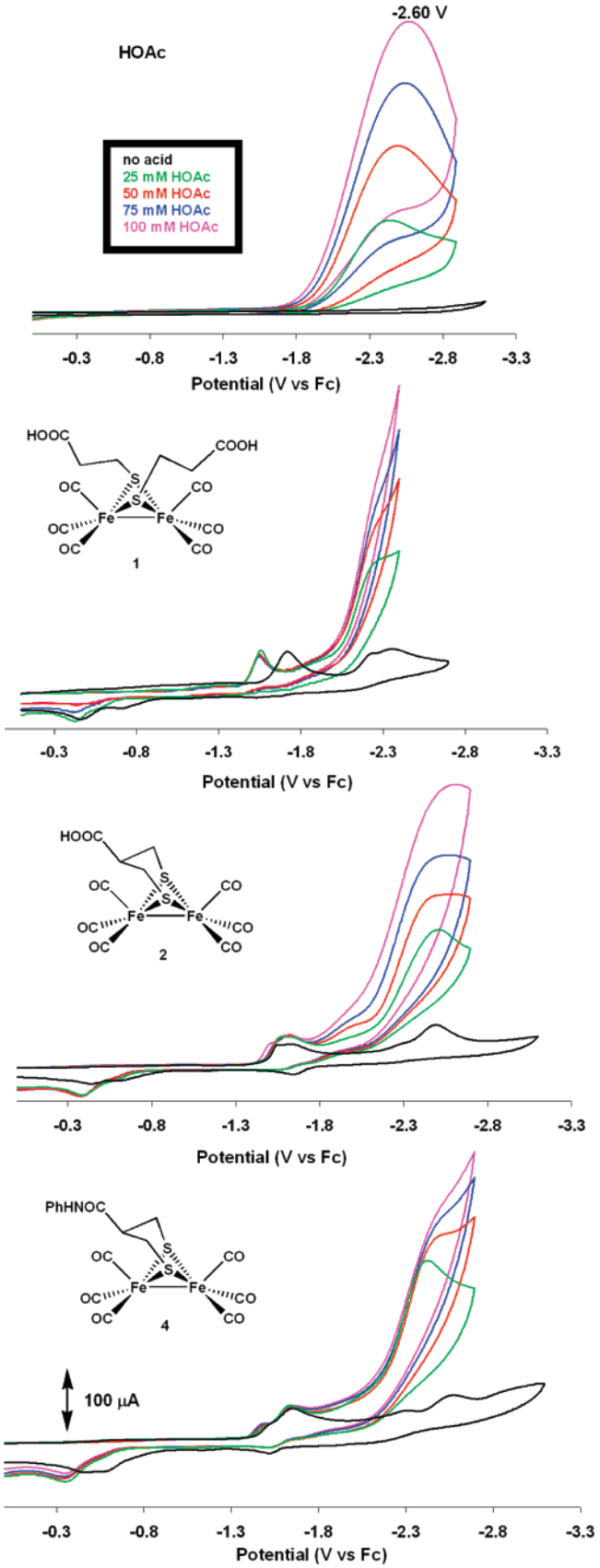

Figure 2. Cyclic voltammograms of complexes **1**, **2**, and **4** (2.5 mM) with HOAc (0, 25, 50, 75, 100 mM) in 0.1 M $^{n}Bu_4NBF_4$ in CO-saturated CH_3CN. The CV of HOAc in MeCN at these concentrations is shown as a control.

species generated at this potential is not active toward electrocatalytic proton reduction (Figure 2). In the case of complex **1**,

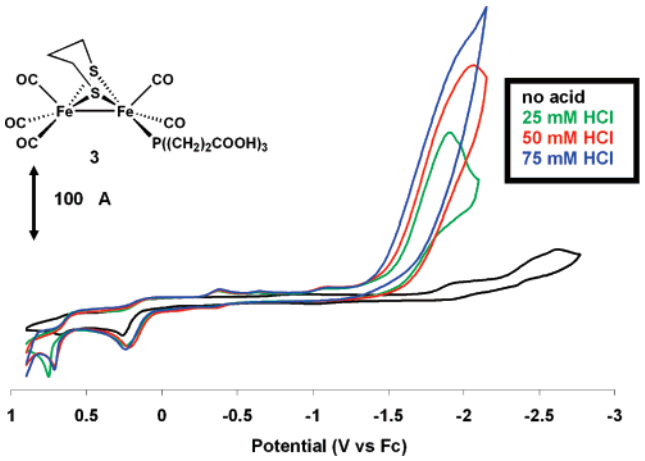

Figure 3. Cyclic voltammograms of **3** (2.5 mM in 0.1 M $^{n}Bu_4NBF_4$ in MeCN under Ar) with increments of HCl (0, 25, 50, and 75 mM).

the potential of the $Fe^{I}Fe^{I}/Fe^{I}Fe^{0}$ couple shifts to more positive potential when acid is added. We postulate that one (or both) of the carboxylic acid moieties is deprotonated in acetonitrile solution and that addition of acid reprotonates the carboxylate and, thus, shifts the reduction potential.[30] The CVs of all three complexes **1**, **2**, and **4** show an increase in current with increasing concentrations of HOAc at or near the second reductive wave (−2.26, −2.51, and −2.43 V, respectively). These values are from 100 to 350 mV more positive than that of acetic acid itself, and the enhanced current is tentatively assigned to the electrochemically generated $Fe^{0}Fe^{0}$ species.

The cyclic voltammogram of the carboxyethyl phosphine complex **3** under an Ar atmosphere has three distinct irreversible reductive features (Figure 3, Table 2). The first reduction at −2.06 V corresponds to a $Fe^{I}Fe^{I}/Fe^{I}Fe^{0}$ couple. It is postulated that the next reduction at −2.44 V is an $Fe^{I}Fe^{0}/Fe^{0}Fe^{0}$ process and that the additional reductive feature at −2.67 V results from the lability of the CO ligand and displacement by MeCN in the $Fe^{0}Fe^{0}$ state, as has been discussed previously in the context of $(\mu\text{-pdt})[Fe(CO)_3]_2$.[8b,31] When increments of HOAc are added, a small increase in peak height is observed for the first reduction of **3**, while the current response of the second reduction increases more dramatically (see Supporting Information). This indicates that for this complex the $Fe^{I}Fe^{0}$ redox state is modestly active toward proton reduction, but the $Fe^{0}Fe^{0}$ state is significantly more catalytically competent. When increments of HCl are added, however, complex **3** becomes a competent electrocatalyst at milder potentials (−1.9 V vs Fc, Figure 3). This positive shift in potential is a result of the stronger acid's ability to protonate **3** more readily in the $Fe^{I}Fe^{0}$ state prior to further reduction to the $Fe^{0}Fe^{0}$ state.

Cyclic voltammetry of the phosphine-substituted complex **5** displays a single one-electron reduction (within the solvent window of MeCN) at −2.42 V (Figure 4). In contrast to the all-CO complexes, complex **5** catalyzes H_2 production from HOAc at this first $Fe^{I}Fe^{I} \rightarrow Fe^{I}Fe^{0}$ event, as has been observed

(30) In support of this hypothesis, monitoring the IR spectrum of **1** in acetonitrile solution reveals that the stretch attributed to the −COOH unit decreases over time, and a new band at ∼1650 cm^{-1} corresponding to $-COO^{-}$ appears (see Supporting Information).

(31) Additional support for this hypothesis is provided by the changes in the relative peak heights of the two reductions at −2.44 and −2.67 V at different scan rates: At faster scan rates (> 500 mV/s), the −2.44 V peak dominates, while the two peak heights are nearly identical at slow scan rates (100 mV/s). See Supporting Information for the corresponding voltammograms.

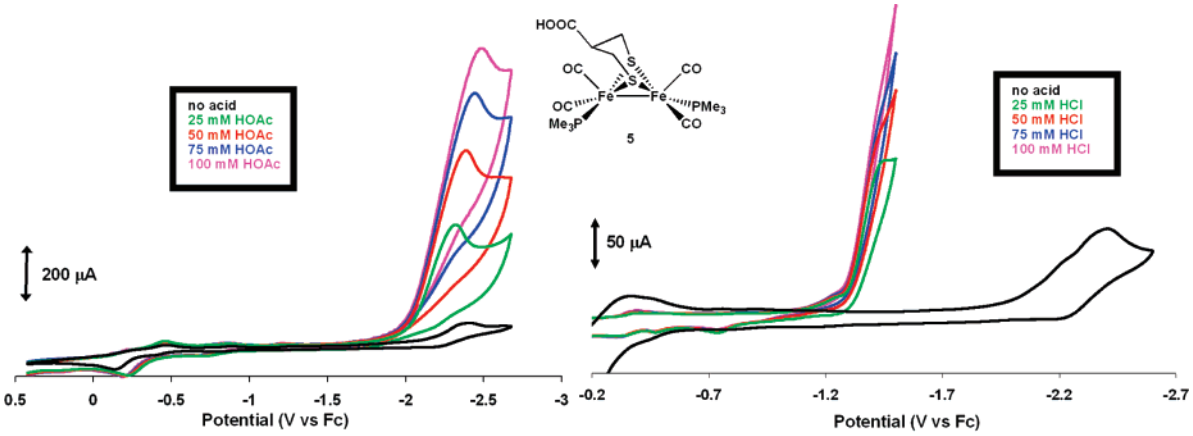

Figure 4. Cyclic voltammograms of **5** (MeCN, 0.1 M ^{n}BuNBF$_4$) in the presence of 0, 25, 50, 75, and 100 mM HOAc (left) and HCl (right).

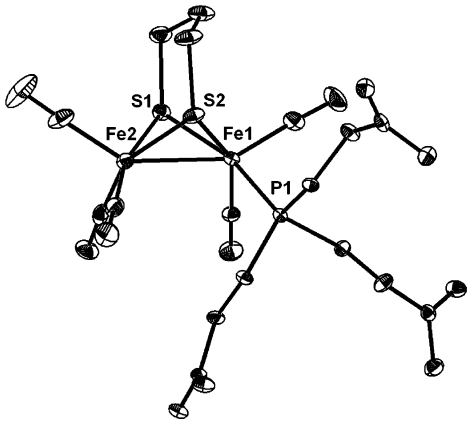

Figure 5. Thermal ellipsoid representation (50% probability) of (μ-pdt)[Fe(CO)$_3$][Fe(CO)$_2${P(C$_2$H$_4$COOH)$_3$}] (**3**). A solvent molecule (H$_2$O) and all hydrogen atoms have been omitted for clarity.

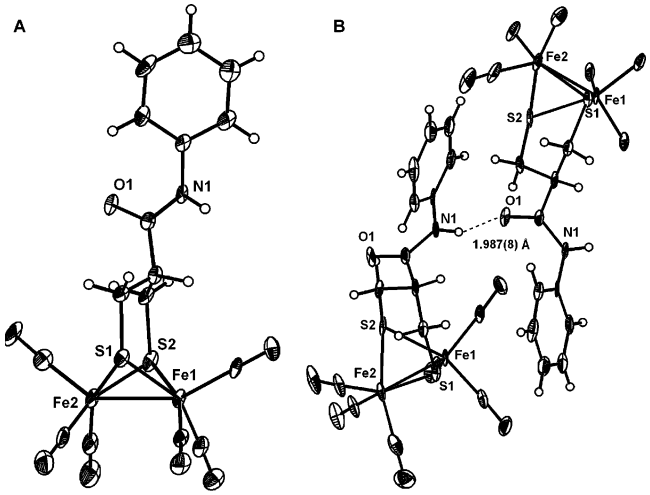

Figure 6. Thermal ellipsoid representation (50% probability) of (μ-(SCH$_2$)$_2$CHCONHPh)[Fe(CO)$_3$]$_2$ (**4**) showing (A) the solid-state structure and (B) hydrogen bonding between two molecules in the unit cell. Solvent molecules (THF) have been omitted for clarity.

for the parent (μ-pdt)[Fe(CO)$_2$(PMe$_3$)]$_2$ complex.[8b] The CV of hydride-bridged Fe^{II}Fe^{II} complex **7** features two irreversible reductive events: a reduction assigned as the Fe^{II}Fe^{II} → Fe^{II}-Fe^{I} process at −1.48 V and a reduction at −2.34 V, coincident with the Fe^{I}Fe^{I} → Fe^{I}Fe^{0} couple of complex **5** (see Supporting Information). Thus, reduction of **7** likely leads to loss of the hydride,[8b] and catalytic H$_2$ production occurs from the product of that hydride loss, i.e., **5** in the presence of HOAc. The cyclic voltammograms of **5** in the presence of varying concentrations of HCl, an acid strong enough to protonate complex **5** to generate hydride **7**, reveal electrocatalytic behavior at a more positive potential coincident with the one-electron reduction of **7**.

Solid-State Structures of 3, 4, and 6. The molecular structure of complex **3** reveals that the carboxyethylphosphine occupies a basal position (Figure 5). As with other monosubstituted Fe$_2$S$_2$ model complexes,[9,10] the boat conformation of the metallodithiacyclohexane ring is oriented toward the phosphine-substituted Fe center. The geometry about each metal center, however, remains unaffected by this seemingly more sterically disfavored frozen orientation. As expected, the packing diagram shows an extensive H-bonding array.

As was found in the molecular structure of **2** as well as its ethylamido derivative[13] the solid-state structure of **4** shows that the aniline-derived carboxyamide moiety is also oriented in the sterically favored equatorial position of the six-membered Fe$_2$S$_2$C$_3$ ring (Figure 6A). The interatomic distances and angles of **4** are very similar to those for **2** (Table 3), with an Fe−Fe distance of 2.514(2) Å. An intermolecular hydrogen-bonding interaction is observed in the extended structure of **4** (Figure 6B) between the amido-carbonyl oxygen atom (O1) of one molecule and the amide hydrogen of another (C═O−HN distance = 1.987(8) Å).

Table 3. Selected Interatomic Distances (Å) and Angles (deg) for Complexes 2, 3, 4, and 6

	2[13]	**3**	**4**	**6**
Fe−Fe	2.5130(8)	2.5553(8)	2.514(2)	2.6017(9)
Fe−S−Fe	67.83(2)	68.67(4)	67.76(7)	70.23(3)
	67.79(3)	69.33(4)	68.06(8)	70.00(3)
S−Fe−S	85.21(3)	85.02(5)	85.06(9)	84.50(4)
	85.06(3)	84.85(5)	85.31(8)	84.50(4)
Fe−P	N/A	2.212(1)	N/A	2.235(1)
				2.246(1)

The solid-state structure of **6** confirms the presence of a methyl ester rather than a carboxylic acid (Figure 7). Since the ester functionality should not affect the overall geometry of the diiron complex, the general structural features of ester complex **6** can be inferred for carboxylic acid complex **7** as well. The bridging hydride of **6** was located in the difference Fourier map and refined.[32] As a result of the protonation of the Fe−Fe bond to form an Fe^{II}Fe^{II} complex, the Fe−Fe distance in **6** is modestly

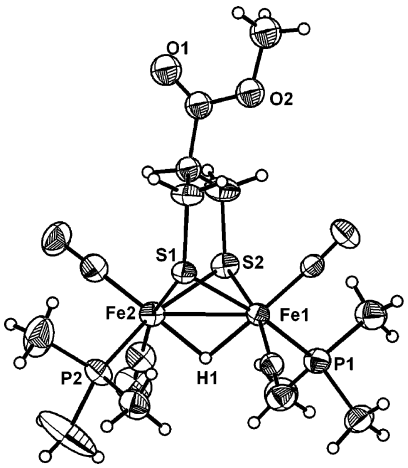

Figure 7. Thermal ellipsoid representation (50% probability) of $\{(\mu\text{-}(SCH_2)_2CHCOMe)(\mu\text{-}H)[Fe(CO)_2(PMe_3)]_2\}PF_6$ (**6**). The PF_6^- counteranion has been omitted.

elongated from the Fe^IFe^I complexes (2.6017(9) Å, compared to ~2.51−2.55 Å). The phosphine ligands both occupy positions *cis* to the bridging hydride. As with the related $\{(\mu\text{-pdt})(\mu\text{-H})[Fe(CO)_2(PMe_3)]_2\}PF_6$ complex,[20] the phosphines are oriented *transoid* to each other.

Conclusions

In summary, diiron dithiolate model complexes of the active site of [FeFe]-hydrogenase bearing carboxylic acid functionalities have been synthesized. We have estabilished that these complexes are spectroscopically and structurally quite similar to their unsubstituted relatives and have comparable electrochemical behavior in solution. In addition, it has been demonstrated that these complexes can undergo the same ligand substitution and protonation processes as their unsubstituted relatives.

The carboxylic acid moieties of these complexes render them amenable to potential applications such as immobilization on electrode surfaces to design heterogeneous electrocatalysts. To mimic the attachment of these complexes to an amino-functionalized electrode surface, $(\mu\text{-}(SCH_2)_2CHCOOH)[Fe(CO)_3]_2$ has been coupled to aniline in solution to generate a carboxyamide linkage. Preliminary attempts to immobilize this complex on an amino-functionalized highly ordered pyrolytic graphite (HOPG) electrode surface have been successful, leading to an electrochemical response very similar to the solution CV data (see Supporting Information). However, the reductive signal does not persist over repeated scans and electrocatalytic proton reduction behavior has not been observed. This limited success may be largely due to the irreversible nature of the reduction of $(\mu\text{-}(SCH_2)_2CHCOOH)[Fe(CO)_3]_2$. It further indicates that additional protective films will be required to maintain stability of such modified electrodes.

Experimental Section

General Considerations. Tetrahydrofuran, methanol, hexanes, acetonitrile, and toluene were degassed and dried by sparging with N_2 gas followed by passage through an activated alumina column. Deuterated solvents were purchased from either Cambridge Isotope Laboratories, Inc. or Aldrich and used without further purification. 2-Carboxy-1,3-propanedithiol[17] and $(\mu\text{-pdt})[Fe(CO)_3]_2$[7a] were prepared using literature methods. All other chemicals were purchased from commercial vendors and used without further purification. NMR spectra were recorded on Varian Mercury and Inova 300 MHz instruments. ^1H NMR chemical shifts were referenced to residual solvent. ^{31}P NMR chemical shifts were referenced to 85% H_3PO_4. Mass spectrometry was performed at the Laboratory for Biological Mass Spectrometry at Texas A&M University. Elemental analyses were performed by Canadian Microanalytical Service in Delta, British Columbia, Canada. Infrared spectra were recorded on a Bruker Tensor 27 instrument using a 0.1 mm NaCl cell.

X-ray Structure Determination. The X-ray data were collected on a Bruker SMART 1000 CCD diffractometer and covered a hemisphere of reciprocal space by a combination of three sets of exposures. The space groups were determined on the basis of systematic absences and intensity statistics. Structures were determined using direct methods with standard Fourier techniques using the Bruker AXS software package.[32] Anisotropic displacement parameters were determined for all non-hydrogen atoms. Hydrogen positions were calculated and refined with fixed isotropic displacement parameters. Crystallographic data are summarized in Table 4.

Electrochemistry. Cyclic voltammetry measurements were performed using a BAS 100A electrochemical workstation. All voltammograms were obtained in a three-electrode cell under Ar (or CO as noted) atmosphere at room temperature. The working electrode was a glassy carbon disk (0.071 cm^2), and a platinum wire was used as the auxiliary electrode. The experimental reference electrode was $Ag/AgNO_3$, and measured potentials are reported relative to the internal reference of $Cp_2Fe/Cp_2Fe^+ = 0.00$. Comparisons to earlier work in CH_3CN solution may be made by adding 0.4 V to the values recorded here. The supporting electrolyte was 0.1 M $^nBu_4NBF_4$. Increments of glacial acetic acid were added by microsyringe.

$(\mu\text{-}SCH_2CH_2COOH)_2[Fe(CO)_3]_2$ (1). Solid $Fe_3(CO)_{12}$ (5.00 g, 10.0 mmol) and 3-mercaptopropionic acid (2.34 g, 22 mmol) were combined in toluene (30 mL) and refluxed under N_2 for 15 min, whereupon the solution color changed from green to red. The reaction mixture was loaded onto a silica column (10 × 1 in.) and eluted first with toluene to remove excess starting materials and then with 1:1 toluene/ethyl acetate to elute the red-orange product. Solvent was removed from the eluant *in vacuo* to yield spectroscopically pure product as a highly insoluble red-orange solid (1.75 g, 35%). Due to the highly insoluble nature of **1**, we were unable to obtain satisfactory ^1H NMR data in any common deuterated solvents. IR (THF, cm^{-1}): ν(CO) 2071 (m), 2037 (s), 1994 (s, br), 1735 (m, COOH). ESI-MS (CH_3CN, neg mode): *m*/*z* 488.79 ($M - H^+$), 460.80 ($M - CO - H^+$). Dec point: 149 °C. Anal. Calcd for $C_{12}H_{10}Fe_2O_{10}S_2$: C, 29.41; H, 2.06. Found: C, 28.99; H, 2.90. Repeated analyses led to similar analytical results; we attribute this to the difficulty in purification arising from the insolubility of this complex.

$(\mu\text{-}(SCH_2)_2CHCOOH)[Fe(CO)_3]_2$ (2). The following is a modification of the literature procedure.[13] Solid $Fe_3(CO)_{12}$ (5.16 g, 10.2 mmol) and 2-carboxy-1,3-propanedithiol (1.56 g, 10.2 mmol) were combined in toluene (30 mL) and refluxed under N_2 for 15 min, whereupon the solution color changed from green to red. The reaction mixture was loaded onto a silica column (10 × 1.5 in) and eluted with toluene to remove excess starting material as a dark green solution. The red-orange product was then eluted with 2:1 toluene/ethyl acetate. Solvent was removed *in vacuo* to yield product as a red-orange microcrystalline solid (2.65 g, 60.5%). IR (THF, cm^{-1}): ν(CO) 2077 (m), 2034 (s), 1992 (s, br), 1978 (sh), 1730 (m, COOH). ^1H NMR (300 MHz, acetone-d_6): δ 3.01

(32) (a) Sheldrick, G. *SHELXS-97*: Program for Crystal Structure Solution; Institut für Anorganische Chemie der Universität: Gottingen, Germany, 1977. (b) *SAINT-PLUS*, version 6.02; Bruker: Madison, WI, 1999. (c) *SHELXTL*, version 6.1; Bruker: Madison, WI, 1998.

Table 4. Crystallographic Data[a] for Complexes 3, 4·THF, and 6

	3·H_2O	**4**·THF	**6**
empirical formula	$C_{17}H_{23}Fe_2O_{12}PS_2$	$C_{20}H_{19}Fe_2NO_8S_2$	$C_{15}H_{27}F_6Fe_2O_6P_3S_2$
fw	626.16	505.08	686.10
cryst syst	triclinic	monoclinic	monoclinic
space group	$P\bar{1}$	$P2_1/c$	$P2_1/n$
unit cell			
a (Å)	8.306(2)	9.701(9)	10.560(3)
b (Å)	8.306(2)	26.87(2)	19.478(5)
c (Å)	19.337(4)	9.429(8)	14.017(4)
α (deg)	98.805(3)	90	90
β (deg)	92.008(3)	104.42(2)	112.13
γ (deg)	117.698(3)	90	90
V (Å^3)	1222.8(4)	2379(4)	2670(1)
Z	2	5	4
d(calcd) (g/cm^3)	1.652	1.762	1.706
R1[b] [$I > 2\sigma(I)$]	0.0508	0.0913	0.0368
wR2[c]	0.1207	0.2188	0.0946

[a] Obtained using graphite-monochromatized Mo Kα radiation ($\lambda = 0.71073$ Å) at 110(2) K for all structures. [b] $R1 = \sum||F_o| - |F_c||/\sum F_o$. [c] $wR2 = [\sum[w(F_o^2 - F_c^2)^2]\sum w(F_o^2)^2]]^{1/2}$.

(dd, $^2J = 16.4$ Hz, $^3J = 3.6$ Hz, 2H, CH_{2ax}), 2.24 (m, 1H, CH), 1.88 (dd, $^2J = 12.9$ Hz, $^3J = 12.6$ Hz, 2H, CH_{2eq}). Dec point: 140 °C.

(μ-pdt)[Fe(CO)$_3$][Fe(CO)$_2${P(C$_2$H$_4$COOH)$_3$}] (3). A solution of Me_3NO (0.578 g, 0.77 mmol) in acetonitrile (5 mL) was added to a solution of (μ-pdt)[$Fe(CO)_3$]$_2$ (0.300 g, 0.77 mmol) in acetonirile (30 mL). After 20 min, tris(2-carboxyethyl)phosphine hydrochloride (0.2207 g, 0.77 mmol) in degassed Mili-Q water was transferred into the solution via cannula. The reaction mixture was stirred at room temperature until IR monitoring indicated that there was no intermediate remaining. After solvent removal *in vacuo*, the solid residue was washed with dry, degassed hexanes (2 × 20 mL) and degassed Mili-Q water (2 × 20 mL). An analytically pure red solid was obtained in a yield of 80%. Crystals suitable for X-ray analysis were grown from a layered ether/hexanes solution. IR (acetonitirile, cm^{-1}): 2041(s), 1981(s), 1966 (sh), 1922 (w), 1733-(w). ^{1}H NMR (300 MHz, acetone-d_6): δ 12.41 (br, 3H, −COO*H*), 2.57(q, 6H, P−CH_2−*CH_2*−), 2.06 (q, 6H, P−*CH_2*−CH_2−), 1.81 (br, 2H, −CH_2−*CH_2*−CH_2−), 1.64 (br, 4H, −*CH_2*−CH_2−*CH_2*−). ^{31}P NMR (121.5 MHz, acetone-d_6): δ 52.89. ESI-MS (CH_3CN, neg mode): m/z 607 (M − H$^+$). Dec point: 144 °C. Anal. Calcd for $C_{17}H_{21}Fe_2O_{11}PS_2$ plus 1 equiv of H_2O: C, 32.61; H, 3.70. Found: C, 32.77; H, 3.57.

(μ-(SCH$_2$)$_2$CHCONHPh)[Fe(CO)$_3$]$_2$ (4). To a stirring solution of **2** (0.5044 g, 1.174 mmol) in THF (20 mL) were added aniline (0.11 mL, 1.2 mmol) and diisopropylcarbodiimide (0.18 mL, 1.2 mmol). The resulting solution gradually changed color from red to orange. After 1 h, the solvent was removed *in vacuo*. The remaining orange solids were washed with hexanes (2 × 20 mL). The solids were then purified by column chromatography (silica, 10 cm), eluting first with toluene to remove impurities, then with 2:1 toluene/EtOAc to elute product. Solvent was removed from the eluant *in vacuo*. The remaining solids were suspended in hexanes (30 mL) and THF was added dropwise until most of the solid had dissolved. This solution was then filtered and cooled to −35 °C overnight to yield analytically pure product as orange needles (0.0945 g, 34%). Crystals suitable for X-ray diffraction were grown via vapor diffusion of hexanes into a concentrated THF solution. IR (MeCN, cm^{-1}): 2078 (m), 2038 (s), 1997 (s, br), 1690 (w), 1600 (w). ^{1}H NMR (300 MHz, acetone-d_6): δ 9.31 (s, 1H, NH), 7.56 (d, $J = 8.4$ Hz, 2H, Ar), 7.27 (m, 2H, Ar), 7.08 (m, 1H, Ar), 3.01 (dd, $J = 39$ Hz, 3 Hz, 2H, CH_{2ax}), 2.36 (m, 1H, CH), 1.99 (m, 2H, CH_{2eq}). Dec point: 130 °C. Anal. Calcd for $C_{16}H_{11}Fe_2NO_7S_2$: C, 38.05; H, 2.20; N, 2.77. Found: C, 38.02; H, 2.01; N, 3.07.

(μ-(SCH$_2$)$_2$CHCOOH)[Fe(CO)$_2$(PMe$_3$)]$_2$ (5). Solid **2** (0.472 g, 1.10 mmol) was dissolved in THF (30 mL). To this was added neat PMe_3 (0.28 mL, 2.8 mmol). The resulting solution was heated to 50 °C for 4 h under N_2, monitoring by IR spectroscopy to ensure that the reaction was complete. Upon cooling to room temperature, volatiles were removed *in vacuo*. The resulting air- and moisture-sensitive red solids were washed with hexanes (2 × 25 mL) and dried *in vacuo* to yield **5** as a red microcrystalline solid (0.458 g, 79.2%). IR (THF, cm^{-1}): 1984 (m), 1948 (vs), 1903 (m), 1729 (w). ^{1}H NMR (300 MHz, acetonitrile-d_3): δ 2.70 (m, 2H, CH_{2ax}), 1.69 (m, 1H, CH), 1.50 (m, 20H, CH_{2eq} and PMe_3). ^{31}P NMR (121.5 MHz, acetone-d_6): δ 27.6 (s, PMe_3), 21.5 (s, PMe_3). Dec point: 108 °C. Anal. Calcd for $C_{14}H_{24}Fe_2O_6P_2S_2$: C, 31.96; H, 4.60. Found: C, 32.22; H, 4.96.

{(μ-(SCH$_2$)$_2$CHCOOMe)(μ-H)[Fe(CO)$_2$(PMe$_3$)]$_2$}PF$_6$ (6). Solid **5** (0.268 g, 0.510 mmol) was dissolved in MeOH (10 mL). To this was added concentrated HCl (10 mL, 12M) dropwise. The solution gradually changed color from dark red to red-orange. After 45 min, an aqueous solution of NH_4PF_6 (0.416 g in 5 mL of H_2O) was added dropwise to precipitate a red-orange solid. Solids were collected via filtration, washed with H_2O (2 × 10 mL) and Et_2O (2 × 20 mL), and dried *in vacuo* to yield analytically pure product (0.260 g, 75.7%). X-ray quality crystals were obtained by cooling a concentrated methanol solution to −35 °C overnight. IR (MeCN, cm^{-1}): 2034 (s), 1994 (s), 1739 (w). ^{1}H NMR (300 MHz, acetone-d_6): δ 3.69 (s, 3H, −COOMe), 3.31 (m, 2H, CH_{2ax}), 2.82 (m, 1H, CH), 2.44 (m, 2H, CH_{2eq}), 1.75 (m, 18H, PMe_3), −15.2 (dd, $^2J_{P-H} = 21$ Hz, 1H, μ-H). ^{31}P NMR (121.5 MHz, acetone-d_6): δ 23.9 (s, PMe_3), 21.7 (s, PMe_3), −142.7 (septet, PF_6). Dec point: 160 °C. Anal. Calcd for $C_{15}H_{27}F_6Fe_2O_6P_3S_2$: C, 26.26; H, 3.97. Found: C, 26.44; H, 3.96.

{(μ-(SCH$_2$)$_2$CHCOOH)(μ-H)[Fe(CO)$_2$(PMe$_3$)]$_2$}PF$_6$ (7). Solid **2** (0.404 g, 0.941 mmol) was dissolved in THF (25 mL). To this was added neat PMe_3 (0.24 mL, 2.4 mmol). The resulting solution was heated to reflux for 4 h under N_2, monitoring by IR spectroscopy to ensure that the reaction was complete. Upon cooling to room temperature, concentrated HCl (20 mL, 12 M) was added dropwise. The solution gradually changed color from dark red to red-orange. After 15 min, a saturated aqueous solution of NH_4PF_6 (10 mL) was added dropwise to precipitate a red-orange solid. Solids were collected via filtration, washed with H_2O (2 × 10 mL) and Et_2O (2 × 20 mL), and dried *in vacuo* to yield product as an orange powder (0.342 g, 54.1%). IR (THF, cm^{-1}): 2032 (s), 1985 (s), 1732 (w). ^{1}H NMR (300 MHz, acetone-d_6): δ 3.34 (m, 2H, CH_{2ax}), 2.79 (m, 1H, CH), 2.44 (m, 2H, CH_{2eq}), 1.71 (m, 18H, PMe_3), −15.2 (t, $^2J_{P-H} = 22$ Hz, 1H, μ-H). ^{31}P NMR (121.5 MHz, acetone-d_6): δ 21.8 (s, PMe_3), 25.1 (s, PMe_3), −142.7 (septet, PF_6). Mp: 162 °C.

Acknowledgment. We acknowledge financial support from the National Science Foundation (CHE-0616695 to

M.Y.D. and CHE-0518047 to M.B.H.) with contributions from the R.A. Welch Foundation (A-0924 to M.Y.D. and A-0648 to M.B.H.). A grant from the Spanish Ministerio de Educación y Ciencia (projects CTQ2006-12097 and CTQ-2005-09105-C04-01) funded Olaf Rüdiger as a visiting scientist to TAMU.

Note added in proof: According to a recent approach to the evaluation of potentials in hydrogen-producing electrocatalysts in non-aqueous solvents (Felton, G. A. N.; Glass, R. S.; Lichtenberger, D. L.; Evans, D. H. *Inorg. Chem.* **2006**, *46*, 9181−9184), the calculated overpotentials for complexes **1**−**5** as electrocatalysts are as follows: **1**, 0.80 V (HOAc); **2**, 1.05 V (HOAc); **3**, 0.98 V (HOAc) 1.24 V (HCl); **4**, 0.97 V (HOAc); **5**, 0.96 V (HOAc) 0.82 V (HCl).

Supporting Information Available: Additional cyclic voltammetry and IR data, and crystallographic tables for **3**, **4**, and **6**. This material is available free of charge via the Internet at http://pubs.acs.org.

OM7003354